Electrophoretic Deposition of Hybrid Calcium Alginate-Gold Nanoparticle Hydrogel Films via Catalyzed Electrooxidation of Hydroquinone

Harikrishnan N. Nambiar and Francis P. Zamborini*

Department of Chemistry, University of Louisville, Louisville, Kentucky 40292, United States

*Corresponding Author

Email: f.zamborini@louisville.edu

ABSTRACT

The electrophoretic deposition (EPD) of hybrid alginate (Alg)-Au nanoparticle (NP) films results from the localized pH drop at the electrode surface due to oxidation of hydroquinone (HQ) catalyzed by 4 and 15 nm diameter citrate-coated gold NPs (cit-Au NPs). The localized pH drop at the electrode leads to neutralization of both Alg and cit, leading to EPD of both Alg and cit-Au NPs simultaneously. Post-treatment of the film with Ca^{2+} solution leads to hybrid Ca-Alg/Au NP hydrogel films. The EPD of Alg in the presence of 4 nm cit-Au NPs occurs at ~0.8 V (vs Ag/AgCl) as compared to ~1.0 V in the presence of 15 nm cit-Au NPs and ~1.4 V in the absence of cit-Au NPs. This is due to the higher catalytic activity of 4 nm cit-Au NPs compared to 15 nm cit-Au NPs for the oxidation of HQ. UV-Vis spectra of Ca-Alg/Au NP hydrogel films show absorbance features for both Ca-Alg and Au NPs entrapped within the hydrogel. As the concentration of Au NPs in the EPD solution increases the Ca-Alg absorbance and localized surface plasmon resonance (LSPR) peak of the Au NPs increases, confirming the role of the Au NPs as a catalyst for EPD of Alg. Attenuated Total Reflectance Fourier Transform Infrared (ATR-FTIR) spectra of the Ca-Alg/Au NP hydrogel films show characteristic peaks for Ca-Alg and protonated alginic acid

groups. The hydrogel thickness is greater with cit-Au NPs compared to without cit-Au NPs at constant EPD potential and time. Forming Ca-Alg and hybrid Ca-Alg/Au NP hydrogel films at low potentials has potential applications in electrochemical and optical sensor development, catalysis, and biological studies.

INTRODUCTION

Metal nanoparticles (NPs) display unique optical, catalytic, and electrochemical properties, which are often different from their bulk metals.[1-3] Properties, such as color,[4] oxidation potential,[5] and surface area-to-volume ratio (SA/V),[6] are highly dependent on their size, shape, and aggregation state,[7] making these properties tunable for specific applications. Since most of the chemical activity occurs at the surface of NPs, the high SA/V allows metal NPs to be more active on a per mole basis in catalytic and sensing applications compared to larger structures.[8-10] In order to explore their unique properties and electrochemical applications, it is important to attach metal NPs onto electrode surfaces. This can be accomplished by using various chemical assembly methods or electrophoretic deposition (EPD).[11, 12]

EPD involves two processes occurring within a two- or three-electrode electrochemical cell. The first process is the migration of charged particles present in the solution/suspension towards the electrode surface under an applied electric field. The second process is the accumulation and deposition of the particles onto the electrode surface.[13-15] EPD offers several advantages over other film formation methods, such as dense packing, high uniformity, predictable kinetics, and controllable kinetics by adjusting EPD parameters.[16] It has been used to deposit many different types of materials and has been extended to deposit charged metal NPs onto conductive surfaces.[17-

[19] For example, Mulvaney *et al.* demonstrated that EPD can be used to assemble thousands of single Au NPs per second into predefined patterned cavities on transparent conductive substrates with nanometer spatial resolution.[20]

The most common mechanism for the EPD process at the electrode-electrolyte interface is charge reduction or neutralization.[11, 13, 21] With this mechanism, a change in pH or ionic strength at the electrode-electrolyte interface leads to destabilization of the surface charge around electrostatically-stabilized NPs, which in turn leads to their deposition. The EPD of particles can occur upon protonation of their negatively-charged basic groups by release of H^+ (pH decrease) at the electrode surface, leading to insolubility and deposition. Release of H^+ ions can occur by electrochemical water oxidation.[11] The problem with this approach is that water oxidation also results in the generation of O_2, which can create bubbles and affect the morphology of the film.[11, 12] This has been overcome by using the oxidation of hydroquinone (HQ) or reduction of benzoquinone (BQ) to deposit negatively-charged basic or positively-charged acidic materials, respectively, by the generation or removal of protons at the electrode, respectively (see Scheme 1). For examples, Sakurada *et al.* deposited zirconia particles by EPD in a bubble free manner by the oxidation of HQ.[22] Zhou *et al.* performed EPD of chitosan using the electroreduction of BQ

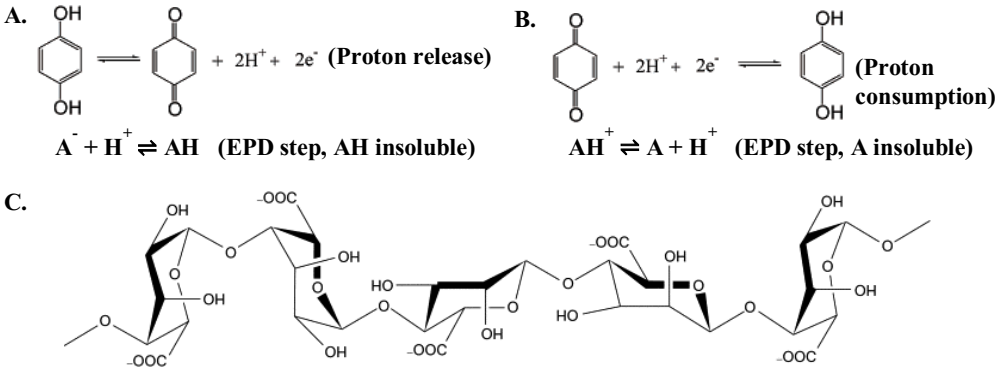

Scheme 1. EPD through **(A)** H^+ release by HQ oxidation and **(B)** H^+ consumption by BQ reduction. **(C)** Chemical structure of alginate. EPD occurs by protonation of COO^- groups.

on an Au electrode and constructed a glucose biosensor by entrapping glucose oxidase and multiwalled carbon nanotubes inside the chitosan film.[23] Liu *et al.* used HQ electrooxidation to co-deposit agarose and a pH responsive small molecule gelator, fluorenyl-9-methoxycarbonyl-phenylalanine (Fmoc-Phe).[24] Our group previously employed HQ oxidation to perform EPD of citrate-stabilized Au NPs (cit-Au NPs) at low potential in a bubble free manner.[11] We observed that smaller cit-Au NPs catalyze HQ oxidation better than larger cit-Au NPs, leading to a lower potential for HQ oxidation and selective deposition of smaller cit-Au NPs.

Alginate (Alg, Scheme 1C) is a naturally occurring biopolymer derived from the cell walls of marine brown algae.[25, 26] It has various properties, including biocompatibility, non-toxicity, high availability, biodegradability, and good adhesive and mechanical properties.[27, 28] Alg is a negatively-charged linear pH shift polysaccharide, which means that it is soluble in basic solution and insoluble in acidic solutions.[29, 30] It is often used to form gels in the presence of calcium ions.[31] Ca-Alg gels have been extensively used to entrap and immobilize enzymes, other proteins, live cells, and NPs at the microscale.[14] Hence Ca-Alg has been successfully used as a matrix for preparing enzyme biosensors, providing good biocompatibility and a favorable environment to retain the enzyme's bioactivity.[32-36] This requires a method to deposit films of Alg in a controlled manner followed by Ca^{2+} cross-linking or deposition of Ca-Alg in one step.

EPD is one method that can be used to immobilize Alg on a suitable electrode surface. Alg EPD allows the co-deposition of other biomolecules or NPs, incorporating them into the electrodeposited Alg films.[37] Several groups have explored the EPD of Alg co–deposited with an enzyme or protein on the electrode surface. For instance, Zhitomirsky and Cheong fabricated a nanocomposite of Alg, hydroxyapatite, TiO_2 and chitosan using EPD on a NiTi (50% Ni) shape memory alloy.[38] Na-Alg was used here for the electro-steric stabilization and charging of ceramic

NPs. Liu *et al.* performed EPD of Na-Alg and horseradish peroxidase on Au electrodes to construct an Alg-based hydrogen peroxide biosensor.[39] The Payne group electrodeposited Ca-Alg on glass/ITO to form hydrogel films and used the method to entrap *E.coli* bacteria without destroying its viability.[31] The entrapped cells were observed to grow and could be liberated from the gels using sodium citrate that out-competed Alg for Ca^{2+} binding, leading to disruption of the Ca-Alg hydrogel. Da Silva *et. al.* used electrodeposition of chitosan, Alg, and poly(3,4-ethylenedioxythiophene)/Alg hybrid hydrogels to form 2D gel patterns on gold plates as well as flexible ITO/polyethylene terephthalate conductive electrodes.[40] EPD of Alg is usually achieved via electrochemical oxidation of water (requires relatively high potential), which creates a localized pH drop that neutralizes the negatively-charged Alg, leading to deposition on the electrode.[31, 38] A major drawback with EPD at higher potentials is that it can denature proteins entrapped in the electrodeposited polysaccharides, causing serious problems for applications.[41] Water electrolysis at higher potentials also affects the conductivity of the electrode surface due to stripping of the ITO layer.[40]

Here we examine the EPD of Na-Alg and negatively-charged cit-Au NPs by proton generation through the oxidation of HQ followed by exposure to Ca^{2+} to form Ca-Alg/Au NP hybrid hydrogel films. This work is unique in that it combines both metal NPs and HQ into the EPD of a charged biopolymer or co-EPD of metal NPs and biopolymer. We observed that the co-EPD of Na-Alg and cit-Au NPs occurs on the electrode surface by Au NP-catalyzed generation of H^+ via electrooxidation of HQ. We previously used HQ for EPD of cit-Au NPs by NP neutralization.[11] Addition of Na-Alg leads to co-EPD of both cit-Au NPs and Alg at low potentials for potentially useful applications.

EXPERIMENTAL SECTION

Chemicals. $HAuCl_4.3H_2O$ was synthesized from 99.9% metallic Au. Acetone (Pharmaco-AAPER, ACS/USP grade), ethanol (Pharmaco-AAPER, ACS/USP grade) and 2-propanol (Sigma Aldrich, ACS reagent) were used as solvents for cleaning Indium-tin-oxide (ITO) - coated glass electrodes (CG-50IN-CUV, R_s = 8-12 Ω). ITO-coated glass slides were purchased from Delta Technologies Limited (Loveland, CO). Alginic acid sodium salt from brown algae (Sigma Aldrich, medium viscosity), sodium borohydride (Sigma Aldrich, ≥ 98.5 reagent grade), trisodium citrate (Bio-Rad laboratories) and hydroquinone (Alfa Aesar) were used as received. NANOpure ultrapure water (Barnstead, resistivity = 18.2 mΩ cm) was used for all aqueous solutions.

Characterization Techniques. UV-Vis spectra were recorded using a Varian instrument model CARY 50 Bio UV-Visible spectrophotometer by scanning between 350 nm to 900 nm wavelength range at a fast scan rate. The background was subtracted using bare glass/ITO as the blank. Infrared spectra were recorded using a Perkin-Elmer Spectrum Fourier Transform infrared spectrophotometer with an attenuated total reflectance attachment. (ATR-FTIR). All dark-field microscopic images were obtained with an inverted Nikon Eclipse Ti microscope with a halogen lamp light source and a dark-field condenser (NA = 0.95-0.80) for sample illumination and a 10x variable aperture. All the EPD experiments were performed on a CH Instruments (Austin, TX) 700E electrochemical workstation.

Synthesis of Au NPs. The established protocols in the literature, as described by our group, previously,[6] were used to synthesize 4 and 15 nm diameter cit–Au NPs. 4 nm cit–Au NPs were synthesized using borohydride reduction[42] of $AuCl_4^-$ in the presence of trisodium citrate while 15 nm diameter cit–Au NPs were synthesized using citrate reduction[43] in a boiling aqueous solution of $AuCl_4^-$. The final concentration of $AuCl_4^-$ in both methods was 0.25 mM. The size of the as-

prepared Au NPs was confirmed using UV–Vis spectroscopy and established electrochemical techniques.[6]

Electrophoretic Deposition (EPD) of Na-Alg and Au NPs using HQ. The experimental set-up utilized three electrodes, including a glass/ITO working electrode (area = 0.6 cm^2), Pt wire counter electrode and an Ag/AgCl (3 M KCl) reference electrode arranged in a triangular pattern with the electrodes spaced approximately 1.5 cm from each other and connected to a CH Instruments (Austin, TX) 700E electrochemical workstation.[11, 12] The conductive side of the glass/ITO electrode faced the reference and counter electrodes. The electrodes were immersed in a solution containing 15 mL of 1% (w/v) Na-Alg solution, 6 mL cit-Au NPs solution (0.25 mM Au), 5 mL 0.1 M HQ and 4 mL H_2O (total volume was 30 mL). The final concentration of Na-Alg, Au NPs and HQ was 0.50% (w/v), 50 μM (in terms of Au) and 16.67 mM, respectively. An electrode potential between 0 and 1 V was applied to the glass/ITO working electrode and held for 30 min. After the EPD protocol, the glass/ITO electrode was removed from the beaker cell, rinsed immediately with copious amounts of 1% NaCl solution, and placed in a 1% (w/v) solution of $CaCl_2.2H_2O$ for 30 min at 4 ^0C.[31] The latter step causes the gelation of Ca-Alg/Au NPs film on the glass/ITO electrode. After this step, we allowed the electrode to air dry for 18 h before further characterization using UV–Vis, ATR–FTIR spectroscopy, and dark field microscopy (DFM).

RESULTS AND DISCUSSION

Figure 1 shows the UV-Vis spectra of glass/ITO/Ca-Alg/Au nanoparticle (NP) films (4 and 15 nm diameter citrate (cit)-stabilized Au NPs) prepared by performing EPD from a solution of 0.5 % (w/v) Na-Alg, 16.67 mM hydroquinone (HQ) and 50 μM cit-Au NPs (or no Au NPs) at different

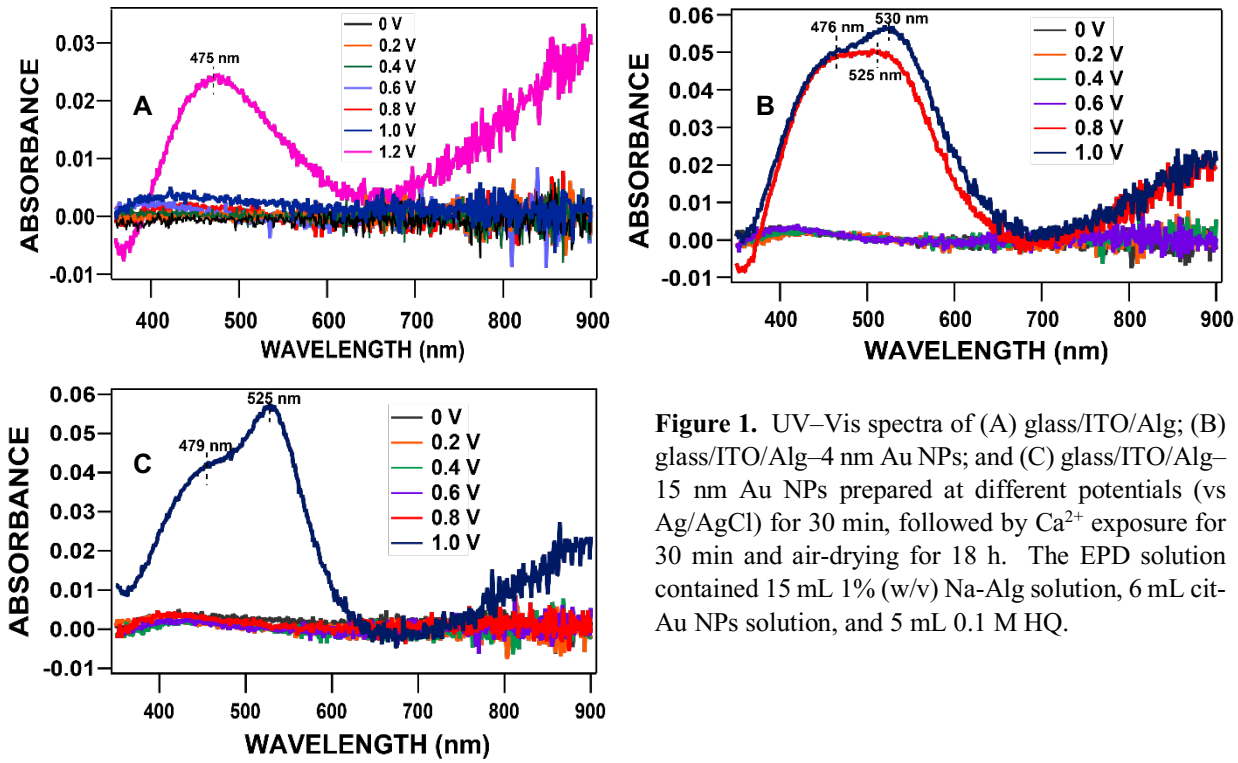

Figure 1. UV–Vis spectra of (A) glass/ITO/Alg; (B) glass/ITO/Alg–4 nm Au NPs; and (C) glass/ITO/Alg–15 nm Au NPs prepared at different potentials (vs Ag/AgCl) for 30 min, followed by Ca^{2+} exposure for 30 min and air-drying for 18 h. The EPD solution contained 15 mL 1% (w/v) Na-Alg solution, 6 mL cit-Au NPs solution, and 5 mL 0.1 M HQ.

potentials for 30 min. Figure 1A shows the UV-Vis spectra of the Ca-Alg hydrogels prepared without cit-Au NPs at potentials ranging from 0 to 1.2 V vs (Ag/AgCl). In the absence of cit-Au NPs, the deposition occurs at 1.2 V vs (Ag/AgCl) as indicated by the presence of a broad band at 475 nm with an absorbance value of 0.025 ± 0.002. This weak band is associated with the Ca-Alg hydrogel since the band at 475 nm (Figure S1-A) is also observed when Ca-Alg hydrogel (Figure S1-B) is prepared by performing EPD at 3 V vs (Ag/AgCl) for 30 min in the absence of HQ and cit–Au NPs. In the presence of 4 nm cit–Au NPs (Figure 1B), the Alg deposited at potentials as low as 0.8 V (vs Ag/AgCl). The localized surface plasmon resonance (LSPR) band[44] for the 4 nm diameter cit–Au NPs trapped in the hydrogel becomes prominent at around 525 nm with a value of 0.054 ± 0.005 (Table S1). A shoulder peak appeared at 476 nm with an absorbance of 0.051 ± 0.003 is related to the Ca-Alg hydrogel formed at the glass/ITO surface. At an EPD potential of 1 V (vs Ag/AgCl), the LSPR band appeared at 530 nm with an absorbance value of 0.065 ± 0.010 and the shoulder peak associated with the hydrogel is at 478 nm with an absorbance value of 0.060

± 0.009. The spectra show that as the EPD potential increases, the amount of 4 nm cit–Au NPs and hydrogel deposited by EPD increases. Moreover, the Au NPs clearly catalyzed the EPD process since the threshold potential in the presence of 4 nm cit–Au NPs was 0.8 V (vs Ag/AgCl) compared to 1.2 V (vs Ag/AgCl) in the absence of the Au NPs. For 15 nm diameter cit-Au NPs (Figure 1C), the threshold potential required to initiate EPD was 1 V (vs Ag/AgCl). At this condition, a strong LSPR band associated with 15 nm diameter cit–Au NPs appeared at 525 nm with an absorbance of 0.064 ± 0.009 (Table S2). The shoulder peak at 479 nm associated with the Ca-Alg hydrogel had an absorbance of 0.042 ± 0.004. As the cit-Au NP size increased from 4 nm to 15 nm diameter, the threshold potential required to initiate EPD increased because the 4 nm diameter cit–Au NPs are more catalytic for HQ oxidation compared to 15 nm diameter cit–Au NPs.[11]

Scheme 2 illustrates the EPD of Alg and negatively charged cit–Au NPs on the glass/ITO electrode through the Au NP catalyzed electrooxidation of HQ. The electrochemical oxidation of HQ at the cit-Au NPs as they impact the glass/ITO generates a localized pH drop at the anode surface.[11, 31] As the concentration of protons increases at the electrode, the negatively-charged COO^- groups of Alg become neutralized (protonated to COOH). The neutralized Alg is insoluble in water, thus allowing it to deposit on the electrode

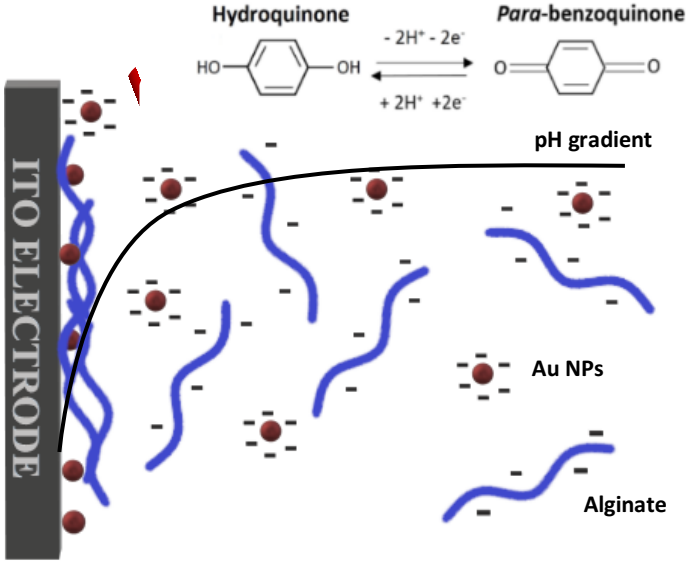

Scheme 2. EPD of Alginate and Au NPs using HQ.

surface. Since the excess protons near the electrode can also neutralize the COO^- groups of citrate, the EPD of cit–Au NPs will also occur simultaneously. We used this approach previously for the EPD of different sized cit–Au NPs by NP charge neutralization.[11] Subsequent exposure to Ca^{2+} leads to the final Ca-Alg/Au NP hydrogel films.

Figure 2 compares the UV-vis spectra of glass/ITO electrodes after EPD of Alg, 4 nm Au NPs only, 15 nm Au NPs only, 4 nm Au NPs + Alg, and 15 nm Au NPs + Alg at 1 V (vs Ag/AgCl) for 30 minutes. Solutions contained 50 μM Au NPs, 16.67 mM HQ, and 0.50 % (w/v) Na-Alg (total volume was 30 mL) when all components were present and at the same concentrations when some components were absent. In the presence of Alg but no cit-Au NPs, the UV-Vis spectra of the glass/ITO electrode showed no significant absorbance. When the Au NPs were present, the glass/ITO showed a strong peak for Ca-Alg hydrogel and a strong LSPR band associated with the NPs around 525 nm. The absorbance associated with the LSPR bands for 4 and 15 nm diameter cit–Au NPs were 0.065 ± 0.010 and 0.064 ± 0.009, respectively (Tables S1 and S2). A shoulder peak appeared around 475 nm alongside due to the Ca-Alg hydrogel with an absorbance of 0.060 ± 0.009 for the hydrogel with 4 nm diameter cit–Au NPs and absorbance of 0.042 ± 0.004 for 15 nm diameter cit–Au NPs. The shoulder peak had a larger absorbance with 4 nm Au NPs compared to 15 nm Au NPs compared to no cit–AuNPs. We also compared the EPD of 4 nm and 15 nm Au NPs in the absence

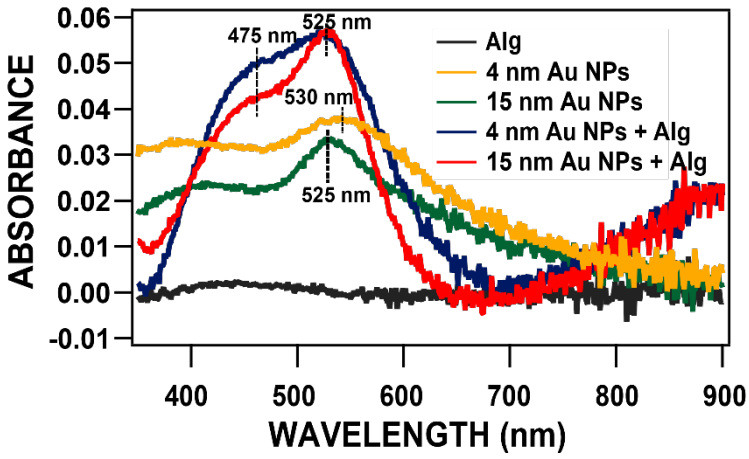

Figure 2. UV–Vis spectra of glass/ITO electrodes after EPD (1 V for 30 min) of Alg, 4 nm Au NPs, 15 nm Au NPs, 4 nm Au NPs + Alg, and 15 nm Au NPs + Alg as indicated, followed by Ca^{2+} exposure for 30 min and air-drying for 18 h.

of Alg, where we substituted Na-Alg for 0.645 mM $NaNO_3$ to keep the ionic strength of the EPD solution constant. The LSPR band for 4 and 15 nm diameter cit–Au NPs deposited at the electrode surface under this condition had absorbances of 0.045 ± 0.003 and 0.033 ± 0.004, respectively. The absorbance values are lower compared to the conditions with Alg present due to the overlap in Alg and Au NP peaks when both are on the surface. The amount of Au NPs deposited with and without Alg present appears to be pretty similar. The spectra for Au NPs without Alg also show a significant absorbance near 480 nm, indicating that the peak at 480 nm when Alg is present is a combination of Au NPs and Alg.

Figure 3 shows dark field microscopy (DFM) images of the cross-section of as-prepared glass/ITO/Ca-Alg or glass/ITO/Ca-Alg/Au NP hydrogel electrodes formed in the presence of 4 nm cit-Au NPs (Figure 3A), in the presence of 15 nm cit–Au NPs (Figure 3B), and in the absence of Au NPs (Figure 3C) after drying the films for 18 hours under ambient temperature and humidity. The darker section with the bright line above it in all images is the glass/ITO electrode as labeled on the images. The faint bright region above the bright line is the Ca-Alg or Ca-Alg/Au NP hydrogel film as labeled. The Ca-Alg/4 nm cit–Au NPs film is an orange color (Figure 3A) while the Ca-Alg/15 nm cit-Au NPs is more of a red color (Figure 3B) with a more intense LSPR band near 530 nm. The Ca-Alg film without any Au NPs appears as a grey color (Figure 3C). Figure

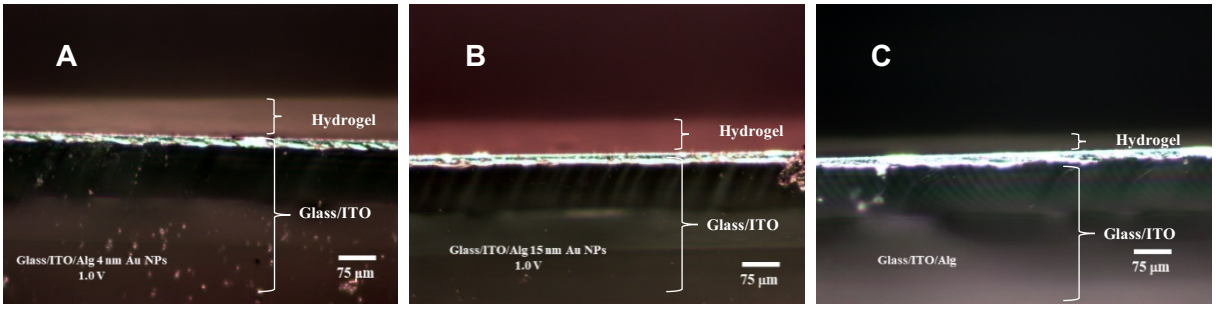

Figure 3. Dark Field Microscopic Images of (A) glass/ITO/Ca-Alg – 4 nm Au NPs, (B) glass/ITO/Ca-Alg – 15 nm Au NPs and (C) glass/ITO/Ca-Alg prepared by EPD at 1 V for 30 min, followed by Ca^{2+} exposure for 30 min and air-drying for 18 h.

S2 shows a cross-section DFM image of glass/ITO without EPD of a Ca-Alg hydrogel film, confirming that the labeling of the Ca-Alg and Ca-Alg/Au NP hydrogel films is correct in Figure 3, as opposed to that region being some type of image artifact. Figure S3 shows DFM images of Ca-Alg/cit-Au NP (4 nm) hydrogel films after air-drying for 5 min and 18 h, revealing the shrinking of the hydrogel film due to water evaporation from the hydrogel. The thickness of the hydrogel films, after soaking in Ca^{2+} for 30 min and air-drying for 18 h, was 72.4 ± 4.6 μm, 67.4 ± 4.7 μm, and 30.0 ± 2.5 μm for Ca-Alg formed with 4 nm Au NPs, with 15 nm Au NPs, and without Au NPs present, respectively. The presence of cit–Au NPs in the EPD solution results in thicker Ca-Alg films, consistent with the Au NPs catalyzing the HQ electrooxidation and increasing the deposition of the Ca-Alg/Au NP films at the electrode surface.

Figure 4 shows ATR–FTIR spectra of the Ca-Alg hydrogels[45] prepared by EPD at 1.0 V for 30 min in the presence and absence of cit–Au NPs, soaking in Ca^{2+} for 30 min, and air-drying for 18 h. The ATR-FTIR spectra are consistent with the literature.[45, 46] The peaks at 3345 cm^{-1}, 1600 cm^{-1} and 1424 cm^{-1}, 1263 cm^{-1} and 1213 cm^{-1}, and 1081 cm^{-1} and 1027 cm^{-1}, correspond to the hydrogen bonded O–H stretch, the asymmetric and symmetric stretching vibrations associated with the COO^- groups (consistent with Ca^{2+}-carboxylates formed), the skeletal vibrations of Alg and alginic acid moieties, and the antisymmetric C–O–C stretching vibration of pyranose rings of the Alg polysaccharide, respectively.[45] The peaks from 750–950 cm^{-1} correspond to various vibrations of the carbohydrate moieties present in the Ca-Alg

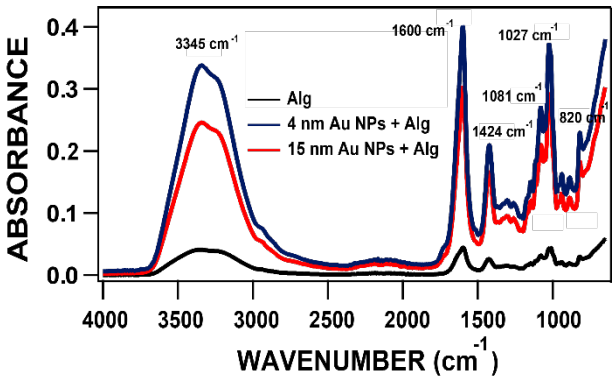

Figure 4. ATR–FTIR spectra of glass/ITO/Alg–Au NPs (4 and 15 nm) as well as glass/ITO/Alg prepared by EPD at 1 V for 30 min, followed by Ca^{2+} exposure for 30 min and air-dried for 18 h.

hydrogel.[45] The absorbance follows the order of Ca-Alg/Au NP (4 nm) > Ca-Alg/Au NP (15 nm) > Ca-Alg. This is consistent with the UV-vis in Figure 2 and DFM in Figure 3, showing significantly greater deposition of Ca-Alg in the presence of Au NPs due to Au NP-catalyzed HQ oxidation. The absorbance from Ca-Alg in the presence of 4 nm Au NPs is slightly higher than 15 nm Au NPs, consistent with Figures 2 and 3. Figure S4 shows the ATR-FTIR spectra of the Ca-Alg hydrogel prepared using EPD with potentials 0.6 V, 0.8 V and 1.0 V, where the absorbance of all peaks (except for O-H stretching at 3345 cm^{-1} due to the presence of water) follows the order 0.6 V < 0.8 V < 1.0 V.

Figure 5 shows plots of Ca-Alg/Au NP hydrogel film absorbance (at 525 nm) and thickness as a function of cit–Au NP concentration for both 4 nm Au NPs and 15 nm Au NPs as determined by UV–Vis spectroscopy (Frames A and B) and DFM (Frames C and D), respectively. As the concentration of cit–Au NPs in the EPD solution increases, the absorbance at 525 nm associated with the LSPR band of the Au NPs increases. For example, when the concentration of 4 nm cit–Au NPs is 25 μM in the EPD electrolyte, the LSPR band (525 nm) had an absorbance value of 0.036 ± 0.007 and a shoulder peak at 475 nm (Figure S5-A) with absorbance of 0.035 ± 0.008. When the concentration of 4 nm cit–Au NPs was 50 μM (2x), the LSPR peak and 475 nm peak (Figure S5-A) increased to 0.065 ± 0.010 and 0.060 ± 0.009, respectively. At 75 μM 4 nm cit–Au NPs, the LSPR and 475 nm absorbance (Figure S5-A) was 0.086 ± 0.017 and 0.077 ± 0.008, respectively. A similar trend occurred for the 15 nm diameter cit–Au NPs. The absorbances of the LSPR peak were 0.046 ± 0.006, 0.064 ± 0.009 and 0.129 ± 0.025 and absorbances of the shoulder peak (Figure S5-B) were 0.033 ± 0.003, 0.042 ± 0.004, and 0.090 ± 0.030 for concentrations of 25 μM, 50 μM, and 75 μM 15 nm cit–Au NPs, respectively. This indicates that the EPD of Alg is heavily influenced by the concentration of Au NPs within the electrolyte

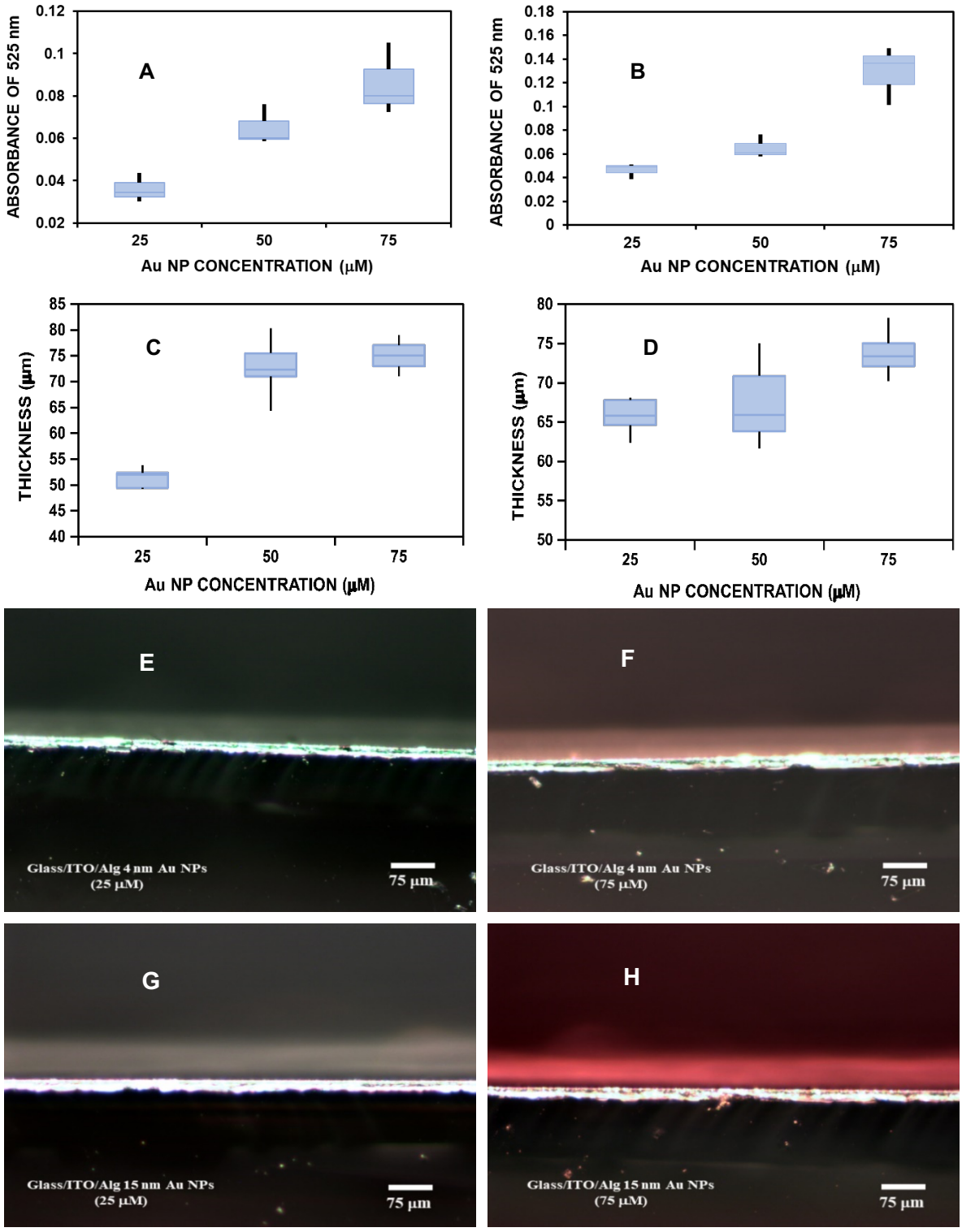

Figure 5. Plots of UV-Vis absorbance at 525 nm vs concentration of the Au NPs in the EPD electrolyte for glass/ITO/Alg-Au NPs containing **(A)** 4 nm Au NPs and **(B)** 15 nm Au NPs; and the thickness measured using DFM vs the concentration of Au NPs in the EPD electrolyte for glass/ITO/Alg-Au NPs containing **(C)** 4 nm Au NPs and **(D)** 15 nm Au NPs; DFM Images of glass/ITO/Alg-Au NPs prepared by EPD at 1 V for 30 min using **(E)** 25 μM and **(F)** 50 μM 4 nm Au NPs, and **(G)** 25 μM and **(H)** 50 μM 15 nm Au NPs, followed by Ca^{2+} exposure for 30 min and air-dried for 18 h.

solution, which is likely due to the increasing number of Au NPs impacting the glass/ITO (flux) as the Au NP concentration increases. More catalytic sites become available for HQ electrooxidation,[11] which in turn increases the concentration of H^+ formed at the electrode surface, resulting in the increased neutralization of Alg and Au NPs.

The measured thicknesses, using DFM, of the hydrogels formed under the above conditions shed light on the influence of the Au NP concentration on EPD. The hydrogel films formed using 25 μM, 50 μM, and 75 μM 4 nm cit–Au NP (Figure 5C) had thicknesses of 51.3 ± 1.8 μm, 72.4 ± 4.6 μm and 75.2 ± 2.8 μm, respectively. The hydrogels prepared using 25 μM, 50 μM, and 75 μM of 15 nm cit–Au NPs (Figure 5D) had thicknesses of 65.8 ± 2.1 μm, 67.4 ± 4.7 μm and 73.9 ± 2.6 μm, respectively. The thickness data also shows that the concentration of cit–Au NPs in the EPD solution influences the final Ca-Alg hydrogel. Figures 5E and 5F show DFM images of Ca-Alg films prepared using 25 μM and 75 μM 4 nm cit–Au NPs. From the images it is evident that as the concentration of Au NPs within the EPD solution increases, the number of NPs entrapped in the hydrogel increased as evidenced by the film color being more pronounced. This also occurred with 15 nm cit–Au NPs, where the color of the hydrogel significantly increased with an increase in the concentration of Au NPs in the EPD solution (Figure 3, 5G and 5H). Since the thicknesses of the films was not dramatically different from 50 μM to 75 μM (Figure 3 and 5H), but the absorbance increased dramatically, we conclude that a greater concentration of Au NPs leads to greater density of Au NPs within the film without a proportionately large increase in thickness.

The concentration of Na-Alg present in the electrolyte also influenced the EPD process (Figure 6 and S6). Figure 6A shows a plot of film absorbance at 525 nm (LSPR band) as a function of Na-Alg concentration with 4 nm diameter cit–Au NPs in the EPD solution. The film absorbances

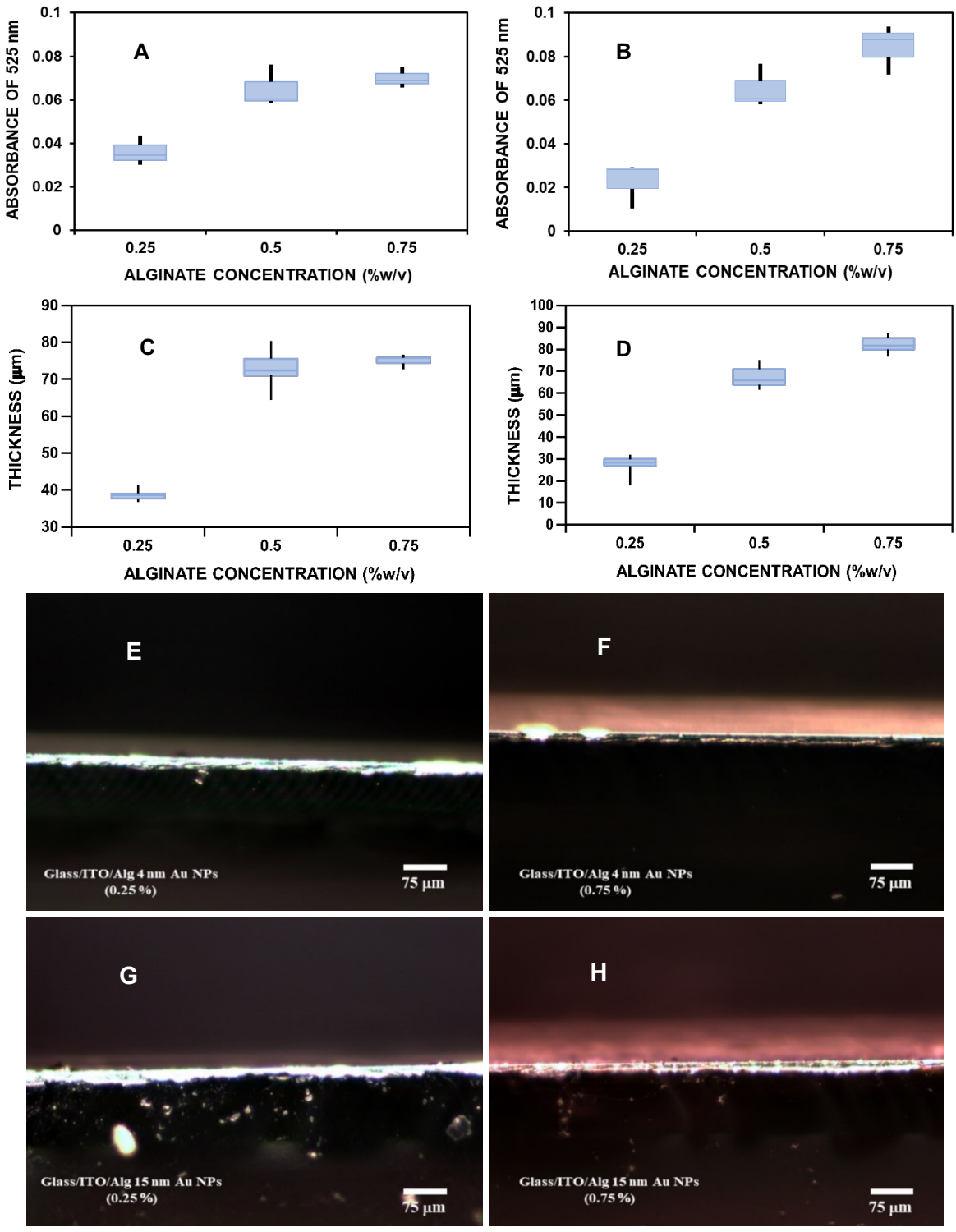

Figure 6. Plots of UV-Vis absorption at 525 nm of the Alg-Au NP films vs concentration of the Au NPs in the EPD solution for glass/ITO/Alg-Au NPs containing (A) 4 nm Au NPs and (B) 15 nm Au NPs. Plot of the thickness measured using DFM vs the concentration of Au NPs in the EPD solution for glass/ITO/Alg-Au NPs containing (C) 4 nm Au NPs and (D) 15 nm Au NPs. Example DFM images of glass/ITO/Alg-Au NPs prepared by EPD at 1 V for 30 min using (E) 0.25% and (F) 0.75% (w/v) Alg and 4 nm Au NPs, and (G) 0.25% and (H) 0.75% (w/v) Alg with 15 nm Au NPs, followed by Ca^{2+} exposure for 30 min and air-dried for 18 h.

at 525 nm were 0.037 ± 0.008, 0.065 ± 0.010, and 0.070 ± 0.005 for concentrations of 0.25%, 0.50%, and 0.75% Na-Alg (w/v), respectively. Figure S6-A shows the absorbances at 475 nm, which were 0.034 ± 0.008, 0.060 ± 0.009, and 0.070 ± 0.005 for concentrations of 0.25%, 0.50%, and 0.75% Na-Alg (w/v), respectively. For 15 nm Au NPs (Figure 6B), the absorbances at 525 nm were 0.023 ± 0.011, 0.064 ± 0.009, and 0.064 ± 0.008 while the absorbances at 475 nm (Figure S6-B) were 0.020 ± 0.009, 0.042 ± 0.004, and 0.057 ± 0.014 for concentrations of 0.25%, 0.50%, and 0.75% Na-Alg (w/v), respectively. The film deposition increased with increasing Na-Alg concentration due to greater mass transfer rate of Na-Alg with increasing bulk concentration.

The thicknesses of the hydrogels prepared using different concentrations of Na-Alg and 4 nm diameter cit–Au NPs (Figure 6C) or 15 nm diameter cit-Au NPs (Figure 6D) showed a similar trend as observed in the UV–Vis spectra. The thicknesses were 38.6 ± 1.3 μm, 72.4 ± 4.6 μm, and 75.1 ± 1.3 μm for Ca-Alg hydrogel films with 4 nm Au NPs prepared using 0.25%, 0.50%, and 0.75% (w/v) Na-Alg, respectively. The thicknesses for Ca-Alg films with 15 nm Au NPs were 27.0 ± 4.7 μm, 67.4 ± 4.7 μm, and 82.3 ± 3.5 μm for 0.25%, 0.50% and 0.75% (w/v) Na-Alg, respectively. Figures 6E and 6F show DFM images for the Ca-Alg/Au NP (4 nm) films prepared with 0.25% and 0.75% (w/v) Na-Alg, respectively. Figures 6G and 6H show the corresponding DFM images for Ca-Alg/Au NP (15 nm) hydrogel films. In both cases the films are clearly thicker, and the color is more pronounced with the larger Na-Alg concentration. A higher concentration of Na-Alg leads to more film material but greater Au NP density as well, as determined by the enhanced color. Interestingly, the thickness increase was not linear with concentration, suggesting that something else may be limiting the film growth. It may be that film density increases with larger Na-Alg concentration but that the thickness is similar. The long drying step also affects the final film thickness (Figure S3).

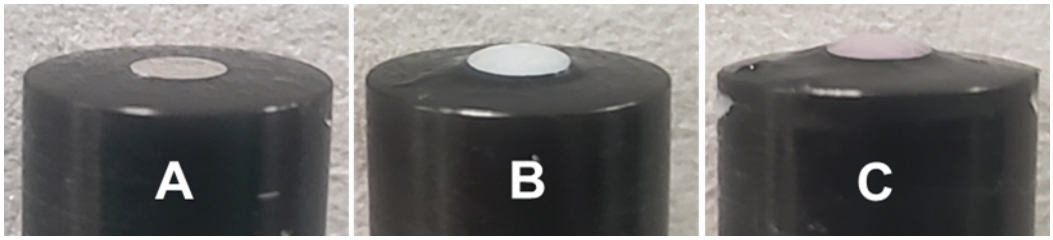

Figure 7. Images of (A) Pt disk electrode, (B) Pt/Ca-Alg, and (C) Pt/Ca-Alg/Au NP (15 nm) hydrogels formed on a 2 mm diameter Pt disk electrode by EPD of Na-Alg in the presence of HQ at 1.4 V and 15 nm Au NPs (C only) for 30 min followed by Ca^{2+} exposure for 30 min and air-drying for 5 min.

Figure 7 shows the Ca-Alg hydrogel deposited on a 25 mm Pt disc electrode using the EPD of Na-Alg (in the presence and absence of 15 nm cit-Au NPs) using HQ electrooxidation at 1.4 V (vs Ag/AgCl) for 30 min, followed by soaking in Ca^{2+} for 30 min, and air-drying for 5 min. This method is suitable to selectively deposit Ca-Alg and Ca-Alg/Au NP films on conductive surfaces, taking on the shape of the conductive material. Here the film formation led to a thick hemispherical Ca-Alg hydrogel on the Pt disc electrode. The EPD of hydrogel/metal NP films onto electrodes could be used as a method to control the size and shape of the hydrogels formed or used to perform electrochemical experiments within the hydrogel, which will be the focus of future experiments.

CONCLUSIONS

Here we described the EPD of Ca-Alg and composite Ca-Alg/Au NP hydrogel films using cit–Au NP-catalyzed electrooxidation of HQ. The oxidation of HQ leads to a local pH decrease at the electrode surface, promoting neutralization and deposition of Na-Alg and cit-Au NPs simultaneously on the electrode surface. This approach has significance as it can lower the EPD potential due to the catalysis of electrooxidation of HQ by cit-Au NPs. The threshold EPD potential was 0.8 V (vs Ag/AgCl) with Na-Alg and 4 nm cit–Au NPs compared to 1.0 V for 15 nm

cit–Au NPs and 1.2 V or greater for Na-Alg with no cit-Au NPs. UV-Vis spectroscopy and DFM showed the role of Au NPs in decreasing the potential and increasing the film thickness of Ca-Alg films. The concentration of cit-Au NPs and Na-Alg during EPD also plays a significant role in the amount of film deposition. ATR-FTIR spectroscopy showed characteristic peaks for the Ca-Alg hydrogel. The absorbance and thickness measured from UV-vis spectroscopy and DFM, respectively, as a function of Au NP concentration and Na-Alg concentration revealed important trends. As Au NP concentration and Na-Alg concentration increased, both absorbance and thickness increased. In the case of Au NPs, the thickness did not increase as much as the absorbance, revealing that the films become more loaded with Au NPs with increasing Au NP concentration versus increasing in thickness. With increasing Na-Alg concentration, the films become thicker with an increase in Au NP concentration indicated by the increase in color of the films. The absorbance is more dominated by the amount of Au NPs due to its large extinction coefficient, whereas the thickness is controlled more by the Na-Alg concentration since it makes up a large percentage of the film material and controls water retention. Our film deposition strategy has great promise for applications in sensors, biological studies, electrocatalysis, and energy relevant research.

ASSOCIATED CONTENT

Supporting Information.

UV-Vis spectra and digital image of Ca-Alg film prepared with no HQ; dark-field microscopy images of glass/ITO and glass/ITO/Ca-Alg-4 nm Au NPs at different drying times; ATR-FTIR spectra of glass/ITO/Ca-Alg-4 nm Au NPs formed at different EPD potentials; box plots showing the effect of Au NP concentration and Na-Alg concentration on film absorbance at 475 nm after

EPD; tables showing all UV-vis absorbance values measured under the different EPD conditions studied (concentration and voltage) for 4 nm and 15 nm Au NPs with Na-Alg.

AUTHOR INFORMATION

CORRESPONDING AUTHOR

*E-mail: f.zamborini@louisville.edu

ACKNOWLEDGMENTS

We gratefully acknowledge the National Science Foundation (NSF) for financial support of this research through grant CHE-2004169.

REFERENCES

1. Zeng, S.; Yong, K.-T.; Roy, I.; Dinh, X.-Q.; Yu, X.; Luan, F., A Review on Functionalized Gold Nanoparticles for Biosensing Applications. *Plasmonics* **2011,** *6*, 491-506.
2. Alim, S.; Vejayan, J.; Yusoff, M. M.; Kafi, A. K. M., Recent Uses of Carbon Nanotubes & Gold Nanoparticles in Electrochemistry with Application in Biosensing: A Review. *Biosens. Bioelectron.* **2018,** *121*, 125-136.
3. Saha, K.; Agasti, S. S.; Chaekyu Kim; Li, X.; Rotello, V. M., Gold Nanoparticles in Chemical and Biological Sensing. *Chem. Rev.* **2012,** *112*, 2739-2779.
4. Piella, J.; Bastús, N. G.; Puntes, V., Size-Controlled Synthesis of Sub-10-nanometer Citrate-Stabilized Gold Nanoparticles and Related Optical Properties. *Chem. Mater.* **2016,** *28*, 1066-1075.
5. Ivanova, O. S.; Zamborini, F. P., Size dependent Electrochemical Oxidation of Silver Nanoparticles. *J. Am. Chem. Soc.* **2010,** *132*, 70-72.
6. Sharma, J. N.; Pattadar, D. K.; Mainali, B. P.; Zamborini, F. P., Size Determination of Metal Nanoparticles Based on Electrochemically Measured Surface-Area-to-Volume Ratios. *Anal. Chem.* **2018,** *90*, 9308-9314.
7. Allen, S. L.; Sharma, J. N.; Zamborini, F. P., Aggregation-Dependent Oxidation of Metal Nanoparticles. *J. Am. Chem. Soc.* **2017,** *139*, 12895-12898.
8. Fenger, R.; Fertitta, E.; Kirmse, H.; Thunemann, A. F.; Rademann, K., Size Dependent Catalysis with CTAB-stabilized Gold Nanoparticles. *Phys. Chem. Chem. Phys.* **2012,** *14*, 9343-9349.
9. Roduner, E., Size Matters: Why Nanomaterials are Different. *Chem. Soc. Rev.* **2006,** *35*, 583-592.
10. Zhou, X.; Xu, W.; Liu, G.; Panda, D.; Chen, P., Size-Dependent Catalytic Activity and Dynamics of Gold Nanoparticles at the Single-Molecule Level. *J. Am. Chem. Soc.* **2010,** *132*, 138-146.
11. Allen, S. L.; Zamborini, F. P., Size-Selective Electrophoretic Deposition of Gold Nanoparticles Mediated by Hydroquinone Oxidation. *Langmuir* **2019,** *35*, 2137-2145.

12. Masitas, R. A.; Allen, S. L.; Zamborini, F. P., Size-Dependent Electrophoretic Deposition of Catalytic Gold Nanoparticles. *J. Am. Chem. Soc.* **2016,** *138*, 15295-15298.
13. Besra, L.; Liu, M., A Review on Fundamentals and Applications of Electrophoretic Deposition (EPD). *Prog. Mater. Sci.* **2007,** *52*, 1-61.
14. Maerten, C.; Jierry, L.; Schaaf, P.; Boulmedais, F., Review of Electrochemically Triggered Macromolecular Film Buildup Processes and Their Biomedical Applications. *ACS Appl. Mater. Interfaces* **2017,** *9*, 28117-28138.
15. Seuss, S.; Boccaccini, A. R., Electrophoretic Deposition of Biological Macromolecules, Drugs, and Cells. *Biomacromolecules* **2013,** *14*, 3355-3369.
16. Avcu, E.; Baştan, F. E.; Abdullah, H. Z.; Rehman, M. A. U.; Avcu, Y. Y.; Boccaccini, A. R., Electrophoretic Deposition of Chitosan-Based Composite Coatings for Biomedical Applications: A Review. *Prog. Mater. Sci.* **2019,** *103*, 69-108.
17. Černohorský, O.; Grym, J.; Yatskiv, R.; Pham, V. H.; Dickerson, J. H., Insight into Nanoparticle Charging Mechanism in Nonpolar Solvents To Control the Formation of Pt Nanoparticle Monolayers by Electrophoretic Deposition. *ACS Appl. Mater. Interfaces* **2016,** *8*, 19680-19690.
18. López, I.; Vázquez, A.; Hernández-Padrón, G. H.; Gómez, I., Electrophoretic deposition (EPD) of Silver Nanoparticles and their Application as Surface-Enhanced Raman Scattering (SERS) Substrates. *Appl. Surf. Sci.* **2013,** *280*, 715-719.
19. Giersig, M.; Mulvaney, P., Preparation of Ordered Colloid Monolayers by Electrophoretic Deposition *Langmuir* **1993,** *9*, 3408-3413.
20. Zhang, H.; Cadusch, J.; Kinnear, C.; James, T.; Roberts, A.; Mulvaney, P., Direct Assembly of Large Area Nanoparticle Arrays. *ACS Nano.* **2018,** *12*, 7529-7537.
21. Tassel, J. J. V.; Randall, C. A., Mechanisms of Electrophoretic Deposition. *Key Eng. Mater.* **2006,** *314*, 167-174.
22. Sakurada, O.; Suzuki, K.; Miura, T.; Hashiba, M., Bubble-Free Electrophoretic Deposition of Aqueous Zirconia Suspensions with Hydroquinone. *J. Mater. Sci.* **2004,** *39*, 1845-1847.
23. Zhou, Q.; Xie, Q.; Fu, Y.; Su, Z.; Jia, X.; Yao, S., Electrodeposition of Carbon Nanotubes-Chitosan-Glucose Oxidase Biosensing Composite Films Triggered by Reduction of p-Benzoquinone or H_2O_2. *J. Phys. Chem. B* **2007,** *111*, 11276-11284.
24. Liu, Y.; Cheng, Y.; Wu, H.-C.; Kim, E.; Ulijn, R. V.; Rubloff, G. W.; Bentley, W. E.; Payne, G. F., Electroaddressing Agarose Using Fmoc-Phenylalanine as a Temporary Scaffold. *Langmuir* **2011,** *27*, 7380-7384.
25. Datta, S.; Christena, L. R.; Rajaram, Y. R. S., Enzyme Immobilization: An Overview on Techniques and Support Materials. *3 Biotech.* **2013,** *3*, 1-9.
26. Siddaramaiah; Swamy, T. M. M.; Ramaraj, B.; Lee, J. H., Sodium Alginate and Its Blends with Starch: Thermal and Morphological Properties. *J. Appl. Polym. Sci.* **2008,** *109*, 4075-4081.
27. Jin, Z.; Guven, G.; Bocharova, V.; Halamek, J.; Tokarev, I.; Minko, S.; Melman, A.; Mandler, D.; Katz, E., Electrochemically Controlled Drug-Mimicking Protein Release from Iron-Alginate Thin-Films Associated with an Electrode. *ACS Appl. Mater. Interfaces* **2012,** *4*, 466-475.
28. Jovanović, Ž.; Stojkovska, J.; Obradović, B.; Mišković-Stanković, V., Alginate Hydrogel Microbeads Incorporated with Ag Nanoparticles Obtained by Electrochemical Method. *Mater. Chem. Phys.* **2012,** *133*, 182-189.
29. Buk, V.; Emregul, E.; Emregul, K. C., Alginate Copper Oxide Nano-Biocomposite as a Novel Material for Amperometric Glucose Biosensing. *Mater. Sci. Eng. C* **2017,** *74*, 307-314.
30. Jian, S.; Liu, X.; Sun, H.; Hou, S., The Electrochemical Studies of Cytochrome C Incorporated in 3D Porous Calcium Alginate Films on Glassy Carbon Electrodes. *RSC Adv.* **2014,** *4*, 6165-6172.
31. Shi, X.-W.; Tsao, C.-Y.; Yang, X.; Liu, Y.; Dykstra, P.; Rubloff, G. W.; Ghodssi, R.; Bentley, W. E.; Payne, G. F., Electroaddressing of Cell Populations by Co-Deposition with Calcium Alginate Hydrogels. *Adv. Funct. Mater.* **2009,** *19*, 2074-2080.

32. Jin, Z.; Harvey, A. M.; Mailloux, S.; Halámek, J.; Bocharova, V.; Twiss, M. R.; Katz, E., Electrochemically Simulated Release of Lysozyme from an Alginate Matrix Cross-linked Iron Cations. *J. Mater. Chem.* **2012,** *22*, 19523-19528.
33. Li, Q.; Sun, H.; Liu, X.; Zhao, X. S., Electroactive Porous Films of Myoglobin within Calcium Alginate. *J. Solid. State. Electrochem.* **2011,** *16*, 1651-1661.
34. Novak, S.; Maver, U.; Peternel, Š.; Venturini, P.; Bele, M.; Gaberšček, M., Electrophoretic Deposition as a Tool for Separation of Protein Inclusion Bodies From Host Bacteria in Suspension. *Colloids Surf. A* **2009,** *340*, 155-160.
35. Xu, J.; Liu, C.; Teng, Y., Direct Electrochemistry and Electrocatalysis of Hydrogen Peroxide using Hemoglobin Immobilized in Hollow Zirconium Dioxide Spheres and Sodium Alginate Films. *Microchim Acta* **2010,** *169*, 181-186.
36. Yang, X.; Kim, E.; Liu, Y.; Shi, X.-W.; Rubloff, G. W.; Ghodssi, R.; Bentley, W. E.; Pancer, Z.; Payne, G. F., In-Film Bioprocessing and Immunoanalysis with Electroaddressable Stimuli-Responsive Polysaccharides. *Adv. Funct. Mater.* **2010,** *20*, 1645-1652.
37. Li, J.; Wu, S.; Kim, E.; Yan, K.; Liu, H.; Liu, C.; Dong, H.; Qu, X.; Shi, X.; Shen, J.; Bentley, W. E.; Payne, G. F., Electrobiofabrication: Electrically based Fabrication with Biologically Derived Materials. *Biofabrication* **2019,** *11*, 032002-032025.
38. Cheong, M.; Zhitomirsky, I., Electrodeposition of Alginic Acid and Composite Films. *Colloids Surf. A* **2008,** *328*, 73-78.
39. Liu, C.; Guo, X.; Cui, H.; Yuan, R., An Amperometric Biosensor Fabricated from Electro-co-Deposition of Sodium Alginate and Horseradish Peroxidase. *J. Mol. Catal.* **2009,** *60*, 151-156.
40. Da Silva, A. C.; Wang, J.; Minev, I. R., Electro-assisted Printing of Soft Hydrogels via Controlled Electrochemical Reactions. *Nat. Commun.* **2022,** *13*, 1353.
41. Bakhshandeh, S.; Amin Yavari, S., Electrophoretic Deposition: A Versatile Tool Against Biomaterial Associated Infections. *J. Mater. Chem. B* **2018,** *6*, 1128-1148.
42. Jana, N. R.; Gearheart, L.; Murphy, C. J., Wet Chemical Synthesis of High Aspect Ratio Cylindrical Gold Nanorods. *J. Phys. Chem. B* **2001,** *105*, 4065-4067.
43. Turkevich, J.; Stevenson, P. C.; Hillier, J., A Study of the Nucleation and Growth Processes in the Synthesis of Colloidal Gold. *Discuss. Faraday Soc.* **1951,** *11*, 55-75.
44. Liu, X.; Xu, H.; Xia, H.; Wang, D., Rapid Seeded Growth of Monodisperse, Quasi-Spherical, CitrateStabilized Gold Nanoparticles via H_2O_2 Reduction. *Langmuir* **2012,** *28*, 13720-13726.
45. Leal, D.; Matsuhiro, B.; Rossi, M.; Caruso, F., FT-IR Spectra of Alginic Acid Block Fractions in Three Species of Brown Seaweeds. *Carbohydr. Res.* **2008,** *343*, 308-16.
46. Lawrie, G.; Keen, I.; Drew, B.; Chandler-Temple, A.; Rintoul, L.; Fredericks, P.; Grøndahl, L., Interactions between Alginate and Chitosan Biopolymers Characteristics using FTIR and XPS. *Biomacromolecules* **2007,** *8*, 2533-2541.

FOR TABLE OF CONTENTS ONLY

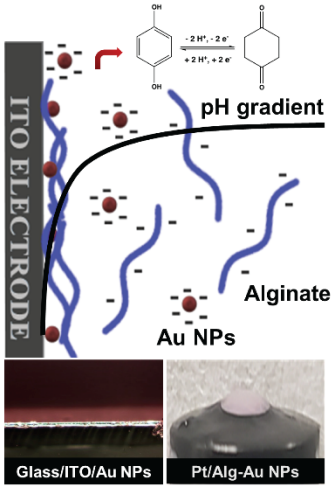
ITO ELECTRODE
pH gradient
Alginate
Au NPs
Glass/ITO/Au NPs
Pt/Alg-Au NPs